J. Fluid Mech. (1985), *vol.* 155, *pp.* 289–307
Printed in Great Britain

Stability of a capillary jet with linearly increasing axial velocity (with application to shaped charges)

By I. FRANKEL† AND D. WEIHS
Department of Aeronautical Engineering, Technion – Israel Institute of Technology, Haifa 32000, Israel

(Received 17 December 1983 and in revised form 14 August 1984)

The stability of a capillary jet of an ideal liquid with a linear variation of axial velocity is investigated. Because of the time dependence in the basic extensional flow the evolution of surface perturbations in the jet is an initial-value problem instead of an eigenvalue one (as in the case of non-stretching jets). The amplification of any given perturbation is found to depend on the relative effects of surface tension and inertia terms associated with the extensional flow as well as on the initial wavenumber and the specific time when the perturbation is introduced in the flow field. The simulation of a shaped-charge jet by the present model is discussed. The results obtained are found to give a good description of the essential features of the breakup phenomenon of such jets.

1. Introduction

The analysis of the stability and breakup of a capillary liquid jet was given by Rayleigh (1894) and extended by Weber (1931) to include the effects of the liquid viscosity and of the aerodynamic pressure distribution in the surrounding gas. Since then it has been extensively studied (Levich 1962; Goldin *et al.* 1969; Bogy 1979) and the classic solutions were extended to include other effects (non-Newtonian fluid, nonlinear effects, the influence of surfactants, etc.).

All the above solutions assumed the jet to move with uniform axial velocity (sometimes even taken to be zero), except for small perturbations. The only analytical investigations of stretching capillary jets were those of Tomotika (1936) which have been revised by Mikami, Cox & Mason (1975). Both these studies neglect the effect of liquid inertia, i.e. they describe creeping flow. The present solution includes for the first time the effects of liquid inertia for an ideal liquid.

We then apply the results of the present solution to the case of the shaped-charge jet, where the high speeds and intense velocity gradients render the creeping-motion approximation inappropriate.

Because of its high penetration capability, the shaped charge has been extensively used since World War II, in both the military and civilian environments. A typical shaped charge consists of an explosive with a conical cavity lined with a thin metal sheet. After the initiation of the charge the liner collapses toward the axis where an extremely high velocity jet is formed (Birkhoff *et al.* 1948).

The velocity of the jet particles increases linearly with the distance from the rear end (Pugh, Eichelberger & Rostoker 1952). Typical velocities are ~ 8 km/s at the tip and ~ 4 km/s at the rear end. Consequently, the jet experiences an enormous stretching during its flight (in typical cases the length can increase by a factor of 4 in 100 μs). This stretching is desirable as it is well known (Birkhoff *et al.* 1948) that the

† Present address: Department of Ocean Engineering, M.I.T. Cambridge, MA 02139.

penetration of the jet is proportional to its length upon impact at the target, which is the reason for designing the charges so as to produce such stretching, highly energetic jets.

We would thus expect the charge to be more effective the greater the distance between the point of production of the jet, and the target (known as the standoff distance). However, beyond a certain standoff distance the stretching jet is broken into a series of closely similar elongated segments during its flight with the result of rapidly deteriorating penetration (Eichelberger 1956; Chou & Carleone 1977; Chou *et al.* 1977).

The jet breakup forms one of the strongest limitations on the penetration capability of shaped charges. The understanding of this phenomenon may thus help in improving the performance of such charges.

In §2 we formulate the problem and derive the characteristic equation, the results of which are presented and discussed in §3. We then apply the results of the stability analysis to the shaped-charge jet in §4.

2. Analysis

Numerous data indicate that the axial velocity of shaped-charge jet particles increases essentially linearly from the rear to the front tip and is not significantly changed from formation to breakup (see e.g. Dipersio, Simon & Martin 1960; Shelton & Arbuckle 1979). We thus neglect the dynamic effects of the jet tips and investigate the stability of an infinitely long capillary cylindrical liquid jet with linearly varying axial velocity. The particles of the jet preserve their axial velocity.

2.1. *The basic solution*

In accordance with the above description we assume W_0, the axial velocity of the jet particles, to be

$$W_0 = Kz_0, \tag{1}$$

where z_0 is the axial (Lagrangian) coordinate of the liquid particle at $t = 0$ and K is the initial strain rate in the jet (see figure 1).

Since $\partial z/\partial t = W_0$, we integrate (1) to find

$$z = z_0(Kt+1), \tag{2}$$

where z is the axial location at time t of a liquid particle, the initial coordinate of which was z_0.

Combining (1) and (2) gives:

$$W_0 = \frac{Kz}{Kt+1}. \tag{3a}$$

Substitution of (3a) into the equation of continuity and integration yield U_0, the radial velocity component,

$$U_0 = -\frac{Kr}{2(Kt+1)}, \tag{3b}$$

where r is the radial coordinate.

The flow field W_0, U_0 in (3a), (3b) is a purely extensional one; thus a circular liquid cylinder whose axis is aligned with z preserves its cylindrical shape (becoming longer and contracting laterally).

Since $\partial r/\partial t = U_0$, we readily obtain

$$r = \frac{r_0}{(Kt+1)^{\frac{1}{2}}},$$

where r_0 is the initial (Lagrangian) radial coordinate of the liquid particle.

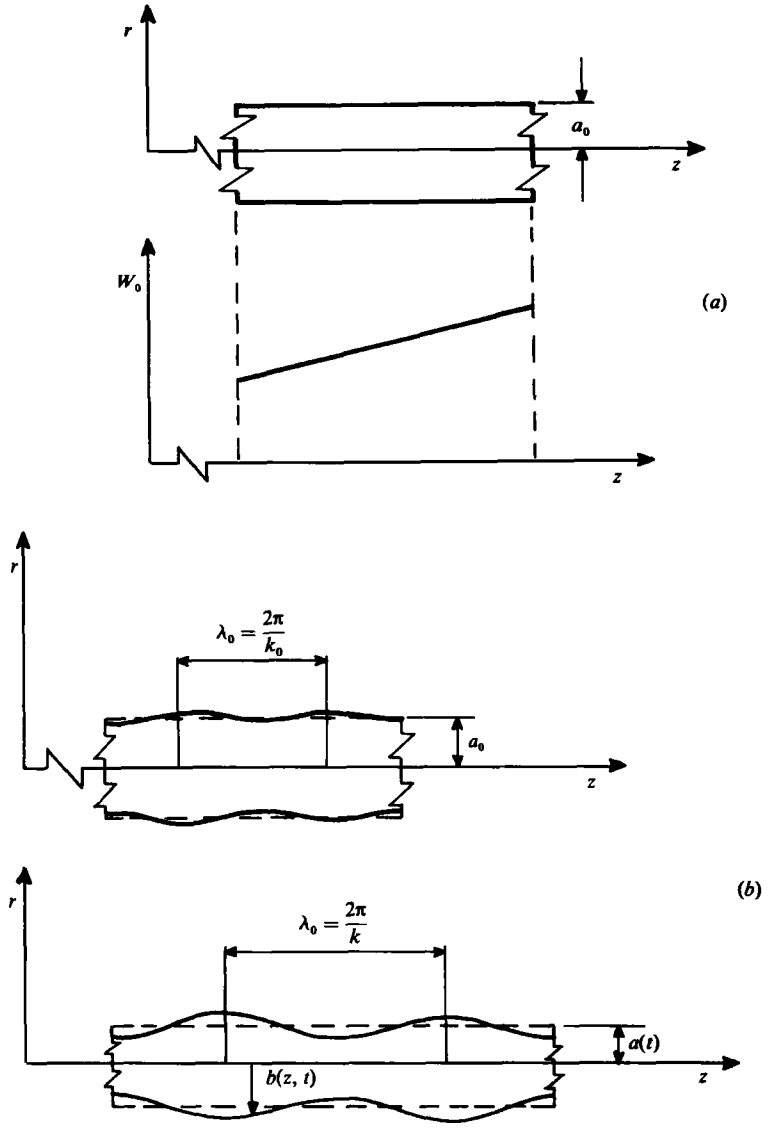

FIGURE 1. (*a*) Schematic description of the jet basic elongational flow field and the coordinate system. (*b*) Schematic description of a typical segment of the stretching jet which is subject to axisymmetric 'varicose' perturbations at non-dimensional time $Kt = 0$ (upper) and $Kt = 0.5$ (lower). ——, the perturbed jet surface $b(z, t)$ ((6) for $m = 0$); ———, the unperturbed radius $a(t)$ (4); $k(\lambda)$ is the wavenumber (wavelength) of the perturbation the initial wavenumber (wavelength) of which is $k_0(\lambda_0)$ (7).

Hence the jet radius is:

$$a(t) = \frac{a_0}{(Kt+1)^{\frac{1}{2}}}, \tag{4}$$

where a_0 is the initial jet radius.

Substitution of the velocity components (3*a*), (3*b*) in Euler's equation and integration gives the pressure distribution in the jet:

$$P_0 = \frac{3}{8}\frac{\rho K^2 a^2}{(Kt+1)^2}\left(1-\frac{r^2}{a^2}\right)+\frac{\sigma}{a}. \tag{5}$$

P_0 satisfies the dynamic boundary condition $P_0 = \sigma/a$ at the jet surface, $r = a$, where σ is the coefficient of surface tension (which is assumed to be constant).

As a result of neglecting the dynamic effects of the jet tips, the basic flow field is one of uniform elongation as if the sections of the jet were moving independently of each other.

2.2. *Stability analysis*

The jet is assumed to be perturbed by small-amplitude standing waves. Neglecting second-order terms in the perturbations we carry out a linear stability analysis.

The perturbed free surface is

$$r = b(\theta, z, t) = a(t)\,[1 + \eta(t)\cos m\theta \cos kz], \tag{6}$$

where $m = 0, 1, 2, \ldots$. The case $m = 0$ describes the axisymmetric 'varicose' perturbation; k is the wavenumber:

$$k = \frac{2\pi}{\lambda} = \frac{k_0}{Kt+1}; \tag{7}$$

and λ is the wavelength. Owing to the basic elongational motion, (3a), the wavenumber decreases as $(Kt+1)^{-1}$ from the initial value k_0 (see figure 1).

$\eta(t)$ is assumed to be a small perturbation $\eta \ll 1$ and thus terms of $O(\eta^2)$ are neglected in the following analysis.

The above form of the perturbation may be considered as a Fourier component in the description of a perturbation with a general spatial (θ, z) dependence. The linearization allows for the stability analysis of each such component separately.

The velocity field in the perturbed jet is:

$$U = U_0 + u; \quad V = v; \quad W = W_0 + w; \tag{8a–c}$$

where U, V, W are the components in the cylindrical coordinate system (r, θ, z) respectively. U_0, W_0 are the velocity components of the basic flow field (3a), (3b) and u, v, w are perturbations, presumably of $O(\eta)$.

The compatibility of the velocity field (8) with the assumed form of the perturbed jet boundary requires that:

$$r = b; \quad U = \frac{\mathrm{D}b}{\mathrm{D}t} = \frac{\partial b}{\partial t} + \boldsymbol{U}\cdot\boldsymbol{\nabla} b. \tag{9}$$

Substitution of U_0, W_0 from (3a), (3b), b from (6), k from (7) and (U, V, W) from (8a) to (8c), neglecting terms of $O(\eta^2)$, results in the kinematic boundary condition:

$$r = a; \quad u = a(t)\,\eta'(t)\cos m\theta \cos kz; \tag{10}$$

where the prime denotes differentiation with respect to the argument.

We define the perturbation potential ϕ as $\boldsymbol{u} = \boldsymbol{\nabla}\phi$ such that ϕ satisfies Laplace's equation $\nabla^2\phi = 0$ within the jet $(0 \leqslant r \leqslant b)$ together with the boundary condition:

$$r = a; \quad \frac{\partial \phi}{\partial r} = a(t)\,\eta'(t)\cos m\theta \cos kz. \tag{11}$$

We look for a solution of the form:

$$\phi = F(r, t)\,G(\theta)\cos kz. \tag{12}$$

Substitution in Laplace's equation, together with the boundary condition (11) and the requirements of regularity at $r = 0$ and single-valuedness results in:

$$\phi = a(t)\,\eta'(t)\,\frac{I_m(kr)}{kI'_m(ka)}\cos m\theta \cos kz; \tag{13}$$

where $I_m(x)$ denotes the modified Bessel function of the first kind and order m of the variable x.

The dynamic boundary condition is:

$$r = b; \quad P = \sigma\left(\frac{1}{R_1}+\frac{1}{R_2}\right) \tag{14}$$

where P is the liquid pressure and R_1, R_2 are the principal radii of curvature of the perturbed jet surface.

From (6) one readily obtains (Lamb 1932, p. 473) to $O(\eta)$:

$$\frac{1}{R_1}+\frac{1}{R_2} = \frac{1}{a}[1-\eta(1-m^2-k^2+a^2)\cos m\theta \cos kz]. \tag{15}$$

The pressure field in the perturbed jet is:

$$P = P_0+p; \tag{16}$$

where P_0, the pressure in the basic flow, is given by (5) and p is the pressure perturbation which is presumably of $O(\eta)$.

Substitution of U_0, W_0 from (3a), (3b), P_0 from (5), U, V, W from (8a) to (8c) and ϕ into Euler's equation, neglecting terms of $O(\eta^2)$ and integrating yields:

$$p = -\rho\left(\frac{\partial\phi}{\partial t}+U_0\frac{\partial\phi}{\partial r}+W_0\frac{\partial\phi}{\partial z}\right). \tag{17}$$

Substituting P_0 from (5), ϕ from (13) and the principal radii of curvature (15), in the dynamic boundary condition (14), neglecting terms $O(\eta^2)$ and employing the modified Bessel equation for I_m:

$$I_m''+\frac{1}{ka}I_m'-\left[\frac{m^2}{(ka)^2}+1\right]I_m = 0,$$

where I_m is a function of ka, we obtain the characteristic equation for $\eta(t)$:

$$\eta''+\frac{K}{2(Kt+1)}\left[3\left(\frac{m^2}{\chi^2}+1\right)\frac{\chi I_m}{I_m'}-2-3\frac{\chi I_m'}{I_m}\right]\eta' - \frac{3}{4}\frac{K^2}{(Kt+1)^2}[T(Kt+1)^{\frac{3}{2}}(1-m^2-\chi^2)-1]\frac{\chi I_m'}{I_m}\eta = 0; \tag{18}$$

where

$$\chi = ka = \frac{k_0 a_0}{(Kt+1)^{\frac{1}{2}}}$$

is the instantaneous non-dimensional wavenumber of a perturbation which had the initial non-dimensional wavenumber $k_0 a_0$ at $t = 0$. (It should be noted that perturbations may be continuously formed in the flow field at all times $t_0 \geqslant 0$, not only at $t_0 = 0$. For perturbations which are introduced at $t_0 > 0$, $k_0 a_0$ is in fact a 'virtual' initial wavenumber which is greater than the actual one χ_0.)

$$T = \frac{4}{3}\frac{\sigma}{\rho K^2 a_0^3},$$

where the non-dimensional parameter T represents the relative effect of the surface tension and the liquid inertia associated with the axial velocity gradient in the basic elongational flow.

The characteristic time for the divergence of perturbations due to the capillary

instability is $\tau_\sigma \sim (\rho a_0^3/\sigma)^{\frac{1}{2}}$ and the characteristic time for the basic elongational flow is $\tau_e \sim 1/K$. Thus:

$$\frac{\tau_e^2}{\tau_\sigma^2} \sim T. \tag{19}$$

In the limiting case $K = 0$ ($T \to \infty$), $\chi = k_0 a_0$ and is no longer a function of t. In this case (18) takes on the form:

$$\eta''(t) - \frac{\sigma}{\rho a_0^3} \frac{k_0 a_0 I_m'(k_0 a_0)}{I_m(k_0 a_0)} (1 - m^2 - k_0^2 a_0^2)\, \eta(t) = 0,$$

which is identical with Rayleigh's classical solution for a capillary non-stretching jet.

A useful alternative form of (18) (for $k > 0$) is obtained by applying the transformation: $\eta(t) = F(\chi)$:

$$3\chi^2 F'' + \left[\frac{3\chi I_m'}{I_m} + 7 - 3\left(\frac{m^2}{\chi^2} + 1\right)\frac{\chi I_m}{I_m'}\right] F' - \left[T\left(\frac{k_0 a_0}{\chi}\right)^{\frac{7}{3}} (1 - m^2 - \chi^2) - 1\right] \frac{\chi I_m'}{I_m} F = 0. \tag{20}$$

3. Results and discussion

As a consequence of the basic elongational flow in the present solution, the wavelength of each perturbation increases with time. Hence the coefficients in (18) and (20) are time dependent and thus the perturbations do not exhibit a simple exponential time dependence.

It is therefore not sufficient to deal with the growth rate of the perturbations (which is not constant) in order to find dominant wavelengths for breakup. We should instead integrate (18) or (20) and follow the time evolution of the perturbations.

Before proceeding to the numerical integration of (18) and (20) we briefly study certain asymptotic cases. These reveal some characteristics of the evolution of perturbations in the elongating jet.

Applying the transformation:

$$F(\chi) = \left(\frac{I_m'}{\chi^{\frac{4}{3}} I_m}\right)^{\frac{1}{2}} G(\chi) \tag{21}$$

to (20), we arrive at:

$$G'' + g(\chi)\, G = 0; \tag{22}$$

where:

$$g(\chi) = -\frac{3}{4}\left(\frac{m^2}{\chi^2} + 1\right)^2 \frac{I_m^2}{I_m'^2} + \frac{1}{3}\left(2\frac{m^2}{\chi^2} + 5\right)\frac{I_m}{\chi I_m'} + \left(\frac{m^2}{2} - \frac{7}{36}\right)\frac{1}{\chi^2} + \frac{1}{2}$$
$$- \frac{1}{3}\left[T\left(\frac{k_0 a_0}{\chi}\right)^{\frac{7}{3}} (1 - m^2 - \chi^2) + 1\right]\frac{I_m'}{\chi I_m} + \frac{1}{4}\frac{I_m'^2}{I_m^2}. \tag{23}$$

The type of asymptotic behaviour of the solutions is related to the sign of $g(\chi)$: If $g(\chi) > 0$ we expect an oscillatory behaviour whereas for $g(\chi) < 0$ some kind of exponential time dependence is to be anticipated (Murray 1974, chap. 6).

For $m \geqslant 1$, $g(\chi) > 0$ for all $\chi > 0$. Only in the axisymmetric case ($m = 0$) does there exist a 'transition point' $\chi = \chi_t$ where $g(\chi)$ changes its sign from $g(\chi) > 0$ for $\chi > \chi_t$ to $g(\chi) < 0$ for $\chi < \chi_t$. Hence the axisymmetric perturbations will be amplified more than all the rest and will dominate the process of jet breakup. (The same conclusion can be reached by transforming (18) in a similar manner.) We therefore limit the following discussion to the case $m = 0$.

The initial development of short-wavelength perturbations can be described by finding an asymptotic solution of (18) for $k_0 a_0 \to \infty$ while $Kt \sim O(1)$. The approximate solution thus obtained† is:

$$\eta \sim (Kt+1)^{\frac{1}{2}} \left\{ A \sin\left[(3\bar{T})^{\frac{1}{2}}\left(\chi^{\frac{1}{2}}+\frac{1}{8\chi^{\frac{3}{2}}}\right)\right] + B\cos\left[(3\bar{T})^{\frac{1}{2}}\left(\chi^{\frac{1}{2}}+\frac{1}{8\chi^{\frac{3}{2}}}\right)\right]\right\}\left[1+O\left(\frac{1}{(k_0 a_0)^{\frac{1}{2}}}\right)\right], \tag{24}$$

where $\bar{T} = T(k_0 a_0)^{\frac{2}{3}}$.

This solution predicts an oscillatory initial behaviour with a moderately increasing amplitude.

The later stages of the evolution of axisymmetric perturbations are approximated by constructing the asymptotic solution of (20) for $\chi \to 0$. The asymptotic procedure yields:

$$F \sim \chi^{\frac{5}{12}} \exp\left[\pm\frac{(6\bar{T})^{\frac{1}{2}}}{\chi^{\frac{1}{6}}}\right]\left[1\mp\frac{15}{8}\frac{\chi^{\frac{1}{6}}}{(6\bar{T})^{\frac{1}{2}}}+O(\chi^{\frac{1}{3}})\right]. \tag{25}$$

Substitution of the expressions for $\bar{T}$ and χ results in:

$$\eta \sim (Kt+1)^{-\frac{5}{8}} \exp\left[(6\bar{T})^{\frac{1}{2}} k_0 a_0 (Kt+1)^{\frac{1}{4}}\right]. \tag{26}$$

The divergence is thus slower than the simple exponential dependence found in the case of capillary non-stretching jets.

Increasing T or $k_0 a_0$ accelerates the divergence: the greater the value of T, the stronger the destabilizing effect of surface tension. $k_0 a_0$ has a similar effect because for a greater $k_0 a_0$ the relevant perturbation reaches the region of small wavenumbers and becomes divergent at a later time when the jet radius is smaller. Therefore this perturbation is built up under a stronger influence of surface tension.

In order to integrate (18) or (20) we need to specify a couple of initial conditions. The choice of the specific values for η, η' is arbitrary. We choose:

$$t = t_0; \quad \eta = 1, \quad \eta' = 0; \tag{27}$$

or:

$$\chi = \chi_0 = \frac{k_0 a_0}{(Kt_0+1)^{\frac{3}{2}}}; \quad F = 1, \quad F' = 0. \tag{28}$$

(The incorporation of other combinations of initial conditions (Appendix A) did not show any essential differences. The above choice is a matter of convenience.)

As argued above, (19), T is a measure of the ratio of the characteristic timescales associated with the basic elongational flow and with the divergence of the unstable perturbations. Hence if $T \gg 1$, the jet breaks up before any significant extension takes place and we may neglect the effects of stretching. On the other hand, if $T \ll 1$, the capillary instability turns out to be very weak. Since we are interested in the description of the jet when both effects are of comparable significance we examine the range $0.1 \leqslant T \leqslant 100$.

Figure 2 shows the variation of the amplitude F with the non-dimensional time Kt (or the instantaneous non-dimensional wave number χ) for $T = 10$ and $k_0 a_0 = 3$.

The two modes of time dependence predicted by the above asymptotic results, (24) and (25), are easily recognized:

Initially, F oscillates with a moderate amplification of amplitude as Kt increases. The amplification is due to the diminishing of the restoring force associated with the surface tension as the wavelength increases with time (as might happen with the

† The details of this and the following asymptotic analyses may be obtained directly from the authors.

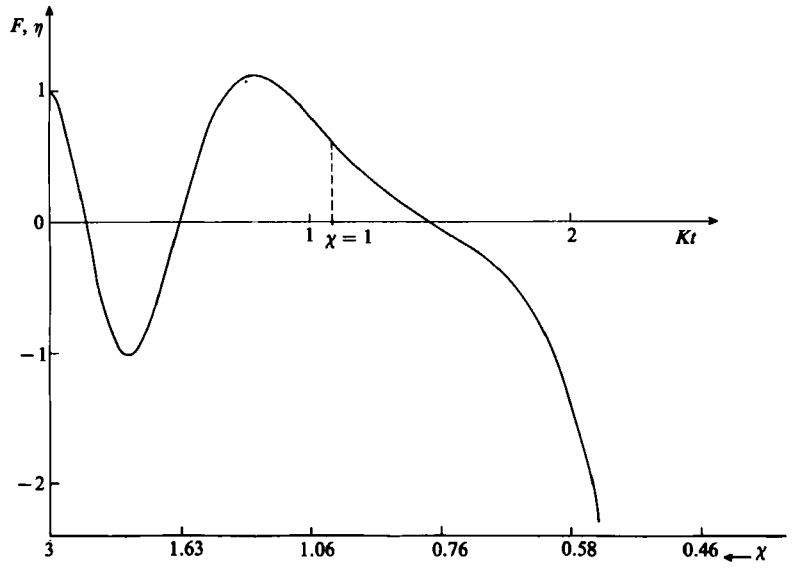

FIGURE 2. Evolution of perturbation amplitude F with non-dimensional time Kt for $T = 10$, $k_0 a_0 = 3$. (The lower scale is χ, the non-dimensional wavenumber.)

vibrations of a mechanical system consisting of a point mass and a spring the 'stiffness constant' of which decreases with time).

As time progresses and χ decreases below $\chi = 1$ the influence of the surface tension becomes destabilizing (the 'stiffness constant' of the spring in the above mechanical model becomes negative). Hence, the turning point which can be seen in the graph shortly after $\chi = 1$, where the curve becomes concave. However, at $\chi = 1$; $F = 0.630$, $F' = 0.310$ ($\eta' = -0.224K$). Owing to the inertia of the liquid, F continues to decrease with decreasing χ (increasing Kt). Only after changing its sign (at $\chi = 0.78$) does it diverge rapidly toward negative values.

In as much as perturbations can form at all times $t_0 \geqslant 0$, $k_0 a_0$ does not represent a single perturbation, but rather the whole spectrum of perturbations the instantaneous wavenumber of which is χ. In order to examine the influence of the time of initiation on the evolution of perturbations figure 3 shows the variation of F with Kt for $T = 10$, $k_0 a_0 = 3$ and $\chi_0 = 3, 2, \chi_c = 0.996, 0.5$. ($\chi_c$ is defined below, (29)). We assume the initial relative amplitude $\eta(t_0)$ ($F(\chi_0)$) to be independent of χ_0.†

For all $\chi_0 > \chi_c = 0.996$ F initially oscillates. For Kt sufficiently large ($Kt > 2$) all the curves diverge, yet the direction of divergence and the values which $|F'|$ attains for a given Kt differ for the different values of $\chi_0(Kt_0)$. The reason for these differences is that the various perturbations reach the region of divergence with different combinations of F, F'. Due to the inertia of the liquid these differences act to delay the divergence in some cases and accelerate it in other cases.

In order to study the influence of the parameters T, $k_0 a_0$ we should therefore select

† Some references (e.g. Mikami *et al.* 1975) assume instead a constant absolute initial perturbation amplitude. The amplification of $\alpha(t)$, the absolute amplitude, is

$$\frac{\alpha(t)}{\alpha(t_0)} = \frac{a(t)}{a(t_0)} \frac{\eta(t)}{\eta(t_0)}.$$

Thus the results obtained for the relative amplitude can be translated in an obvious manner to give the relevant information concerning the absolute amplitude.

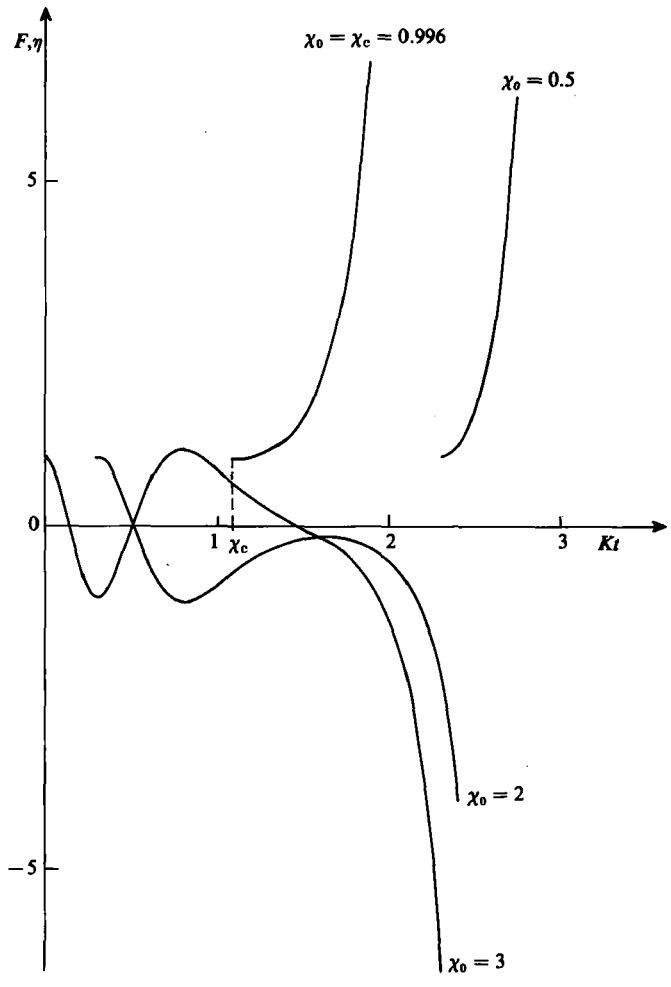

FIGURE 3. Same as in figure 2, but for perturbations introduced at $\chi_0 = 3, 2$, $\chi_c = 0.996, 0.5$.

a certain perturbation from the whole spectrum of perturbations which belong to a given value of $k_0 a_0$. We found it most convenient to choose the earliest perturbation which grows monotonically. From (20) together with the initial conditions, (27), it can be verified (Appendix B) that this condition is satisfied by $\chi_0 = \chi_c$, where χ_c is the solution of:

$$\chi_c^{\frac{1}{2}} + \bar{T}\chi_c^2 - \bar{T} = 0. \tag{29}$$

It is readily shown that for:

$$(k_0 a_0)^2 \leqslant 1 - \frac{1}{\bar{T}}; \tag{30}$$

$k_0 a_0 \leqslant \chi_c$, in which case the whole spectrum of perturbations associated with $k_0 a_0$ grows monotonically. Hence we choose:

$$\chi_0 = \min(\chi_c, k_0 a_0). \tag{31}$$

This choice filters the 'noise' associated with the oscillations prior to χ_c. Apart from this matter of convenience χ_c is of some practical importance in the context of shaped

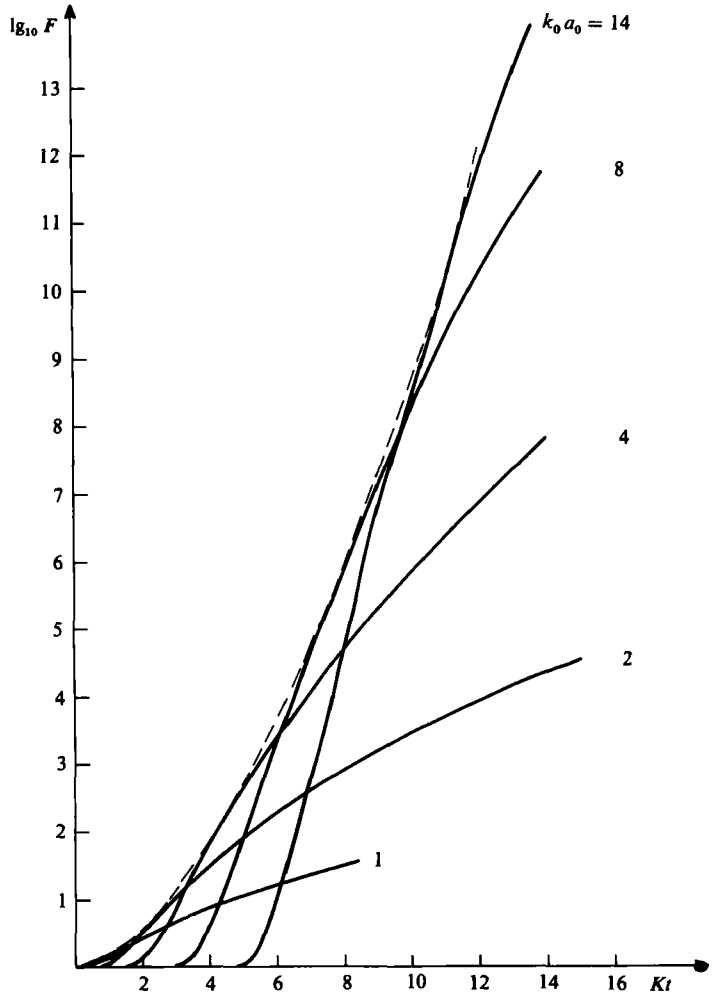

FIGURE 4. Logarithmic amplification $\lg_{10} F$ of perturbations with initial conditions at $\chi_0 = \min(\chi_c, k_0 a_0)$ for $T = 10$ and $k_0 a_0 = 1, 2, 4, 8, 14$. The broken line marks the 'amplification envelope'.

charge design: There is no significant growth of perturbations in the range $\chi > \chi_c$.† Keeping in mind that the timescale for the shaped-charge jet is usually less than 100 μs, certain divergent perturbations may prove practically unimportant since their χ_c is not reached until the jet hits the target.

Figure 4 describes the dependence of $\lg_{10} F$, the logarithmic amplification of the above chosen perturbations, on Kt, the non-dimensional time for $T = 10$, and several values of $k_0 a_0$.

The various curves show slow initial divergence (as could be anticipated since both F' and F'' vanish simultaneously if $\chi_0 = \chi_c$); the growth rate then rapidly increases and is later gradually moderated.

† The amplification of the oscillations in the range $\chi > \chi_c$ appears to be quite moderate. Furthermore, the liquid viscosity (which is not included in the present model) tends to attenuate these early oscillations, if not cancel them altogether (Frankel 1984).

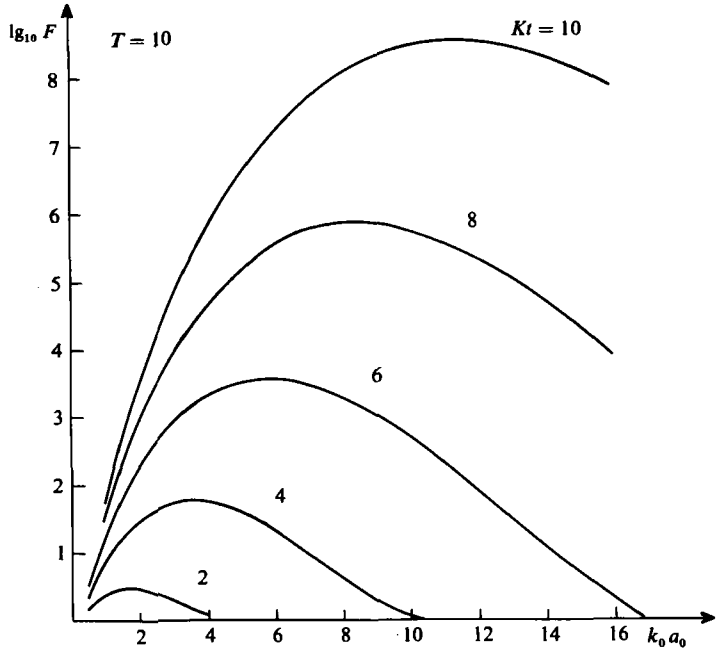

FIGURE 5. The logarithmic amplification $\lg_{10} F$ vs. $k_0 a_0$ for $T = 10$ and $Kt = 2, 4, 6, 8, 10$.

We may further note that, the greater the value of $k_0 a_0$, the greater the amplification of the relevant perturbation, and the later this amplification appears. Consequently, there is no one dominant perturbation throughout the process, but rather at each moment there is a different dominant perturbation.

Figure 5 illustrates the variation of the logarithmic amplification with $k_0 a_0$ for $T = 10$ and several values of the non-dimensional time Kt. This figure shows that the amplification and $(k_0 a_0)_m$, the value of $k_0 a_0$ which belongs to the most amplified perturbation at a given time, are both increased as Kt increases.

Figure 6 shows the variation of the maximal amplification with time for $T = 0.1$, 1, 10, 100. The curve for $T = 10$ is identical with the 'amplification envelope' marked by the broken line in figure 4 (the other curves are obtained in a similar manner). We see that the higher the value of T the greater the amplification for a given Kt. This is quite obvious, since a greater value of T means a stronger destabilizing effect of surface tension.

We now turn to look for the perturbations of maximum amplification assuming that these perturbations are likely to dominate the process of jet breakup. χ_m, the instantaneous non-dimensional wavenumber of the perturbation of maximum growth for given values of T, Kt may be obtained from:

$$\left(\frac{\partial F}{\partial \chi}\right)_{T,\, Kt\,-\,\text{const}} = 0. \tag{32}$$

Since the analytical expression for F is not known, χ_m has to be found numerically. Some insights into the behaviour of the solutions might be gained by first approximating χ_m for $Kt \ll 1$ and $Kt \gg 1$.

(i) For $Kt \ll 1$:

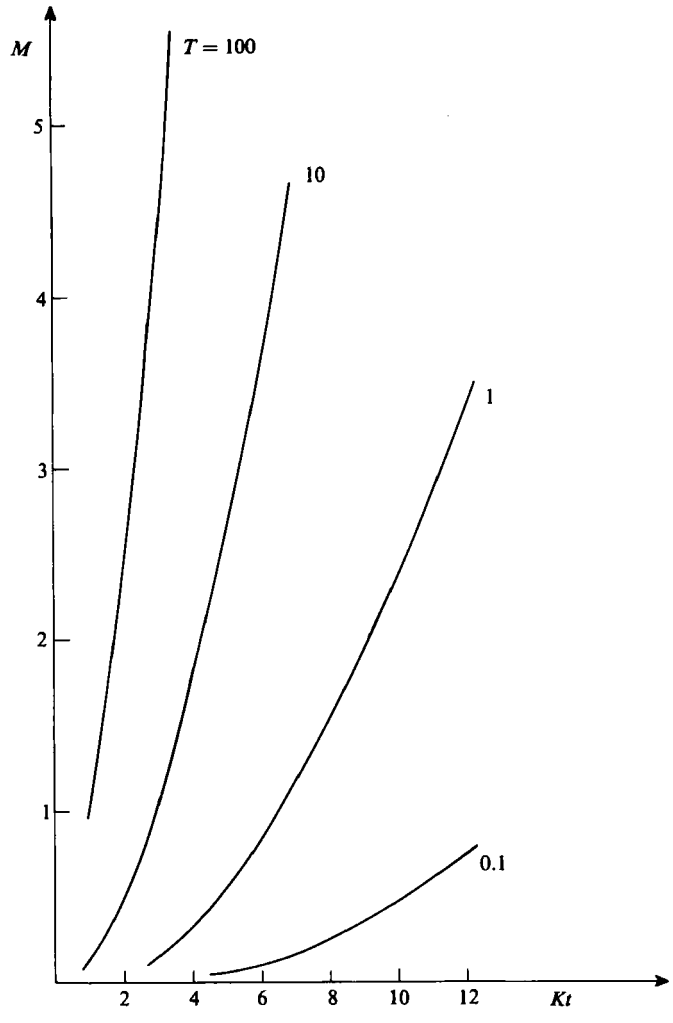

FIGURE 6. Amplification envelopes (time dependence of maximal logarithmic amplification M) for $T = 0.1, 1, 10, 100$.

As η, η' at $t = 0$ are dictated by the initial conditions the small-time behaviour is governed by $\eta''(0)$. $\eta(t)$ may be approximated by:

$$\eta(t) \sim 1 + \tfrac{1}{2}\eta''(0)\, t^2 + O((Kt)^3).$$

Substituting the initial conditions, (27), we obtain from (18):

$$\eta''(0) = \left\{\tfrac{3}{4}K^2[T(1-\chi^2)-1]\frac{\chi I_1}{I_0}\right\}_{\chi = k_0 a_0}. \tag{33}$$

In order that a perturbation may grow at early time $Kt \geqslant 0^+$ we require that $\eta''(0) > 0$, hence:

$$(k_0 a_0)^2 < 1 - \frac{1}{T}, \tag{30}$$

(which assures that $k_0 a_0 < \chi_c$). This inequality cannot be satisfied by any real $k_0 a_0$ unless $T > 1$. It can be readily verified with the aid of (29) that if $T < 1$: $k_0 a_0 > \chi_c$ for any $k_0 a_0 > 0$ and thus it takes a finite time before any perturbation grows.

T	1.01	1.1	1.3	1.5	1.7	3	10	100	1000
χ_{m1}	0.071	0.211	0.338	0.406	0.451	0.572	0.662	0.694	0.697
χ_{m2}	0.099	0.212	0.340	0.406	0.451	0.571	0.661	0.693	0.696
(Kt)	0.0087	0.0035	0.0029	0.0020	0.0020	0.0017	0.0011	0.0006	0.0004

TABLE 1. The dominant perturbations for $Kt \ll 1$, where: χ_{m1} are the asymptotic results obtained from (34); χ_{m2} the numerical computation; and (Kt) the relevant values of Kt at which χ_{m2} was obtained

The perturbation of maximal growth is obtained through:

$$\frac{\partial}{\partial\chi}\left\{[T(1-\chi^2)-1]\frac{\chi I_1}{I_0}\right\}_{\chi=\chi_m} = 0. \tag{34}$$

For $T\to\infty$ we get Rayleigh's solution $\chi_m = 0.697$. The values of χ_m for finite values of $T > 1$ appear in table 1.

(ii) For $Kt \gg 1$:

Since χ_m is determined through the interplay of the surface tension and the inertia of the liquid, it must remain finite. (The destabilizing effect of the surface tension is evidently limited to $\chi < 1$. Due to the inertia effect χ_m must remain finite because the amplification of a perturbation $\chi\to 0$ is associated with the acceleration of an infinite liquid mass). We may thus conclude that, for $Kt \gg 1$, $(k_0 a_0)_m \gg 1$ (and thus $\bar{T} \gg 1$ too).

Consequently we approximate F by looking for an asymptotic solution of (20) for $k_0 a_0\to\infty$ and $\chi < 1$. The expression thus obtained is:

$$F \sim \left(\frac{I_1}{\chi^{\frac{4}{3}}I_0}\right)^{\frac{1}{2}}\frac{1}{[\Phi_0(\chi)]^{\frac{1}{4}}}\left\{A\exp\left[-\bar{T}\int_\chi^1[\Phi_0(\chi')]^{\frac{1}{2}}\,d\chi'\right] + B\exp\left[\bar{T}\int_\chi^1[\Phi_0(\chi')]^{\frac{1}{2}}\,d\chi'\right]\right\}\left[1+O\left(\frac{1}{\bar{T}^{\frac{1}{2}}}\right)\right]; \tag{35}$$

where:
$$\Phi_0(\chi) = \tfrac{1}{3}(1-\chi^2)\frac{I_1}{\chi^{\frac{10}{3}}I_0}. \tag{36}$$

The coefficients A, B should be determined through the application of the initial conditions (28) with χ_0 given by (31). Yet, for $\bar{T} \gg 1$ one readily obtains:

$$\chi_c \sim 1+O\left(\frac{1}{\bar{T}}\right).$$

$\Phi_0(\chi) = 0$ for $\chi = 1$ and F is singular there. This difficulty is circumvented by first finding an approximate solution which is valid in the neighbourhood of $\chi = 1$ and then matching it with the expression in (35).

This procedure yields $B \sim 1/(k_0 a_0)^{\frac{7}{16}}$, $A = (\frac{1}{2}\sqrt{3})B$. Hence the first term in brackets in (35) is negligible for $\bar{T} \gg 1$. Substituting B and expressing $k_0 a_0$ as $(Kt+1)^{\frac{3}{2}}$ we obtain from (35):

$$F \sim H(\chi)\exp\chi^{\frac{7}{4}}(Kt+1)^{\frac{7}{4}}\int_\chi^1[\Phi_0(\chi')]^{\frac{1}{2}}\,d\chi'; \tag{37}$$

where:
$$H(\chi) = \frac{1}{\chi^{\frac{31}{16}}}\left(\frac{I_1}{I_0}\right)^{\frac{1}{2}}\frac{1}{[\Phi_0(\chi)]^{\frac{1}{4}}}.$$

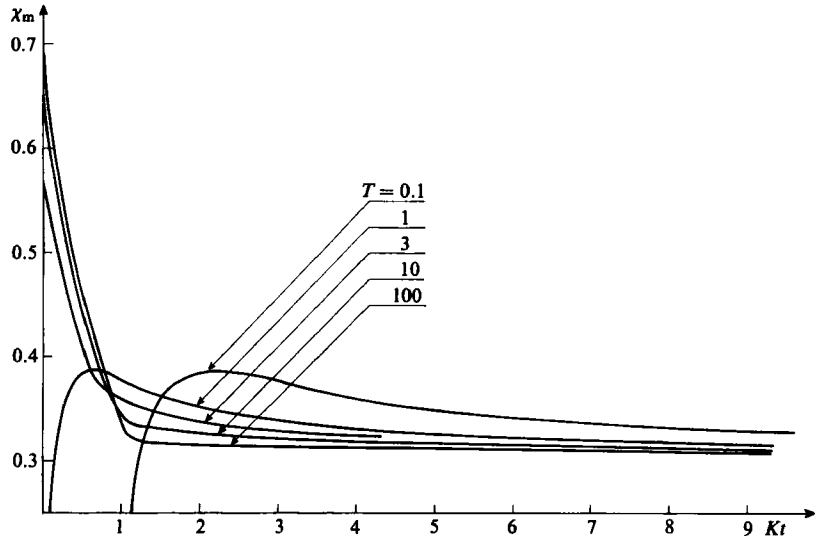

FIGURE 7. Time dependence of χ_m, the non-dimensional wavenumber of dominant perturbations for $T = 0.1, 1, 10, 100$.

Differentiation and substitution in (32) results in

$$\frac{dH}{d\chi}+(Kt+1)^{\frac{7}{4}}\frac{d}{d\chi}\left\{\chi^{\frac{7}{6}}\int_{\chi}^{1}[\Phi_0(\chi')]^{\frac{1}{2}}\,d\chi'\right\}\simeq 0.$$

For $Kt \gg 1$ we may neglect the first term and thus χ_m is the solution of:

$$\frac{7}{6}\int_{\chi_m}^{1}[\Phi_0(\chi')]^{\frac{1}{2}}\,d\chi'-\chi_m[\Phi_0(\chi_m)]^{\frac{1}{2}}=0. \tag{38}$$

Substituting $\Phi_0(\chi)$, from (36), we solve numerically to find $\chi_m = 0.307$ for all T, $Kt \gg 1$.

Figure 7 illustrates the dependence of χ_m on Kt for several values of T. We note that as Kt increases the various curves converge and χ_m tends to a constant limit. The convergence to the limiting value is faster the greater the value of T. For example: at $Kt = 9$ we find that for $T = 0.1, 1, 10, 100$: $\chi_m = 0.329, 0.317, 0.310, 0.308$ respectively (compared with the asymptotic prediction $\chi_m = 0.307$).

For decreasing values of Kt the different curves disperse: the greater T the higher the relevant χ_m. Table 1 compares the results of the numerical computation for $Kt \to 0$ with the asymptotic values obtained from (34). Because of reasons inherent in the numerical procedure χ_m cannot be computed for $Kt = 0$, but only for small $Kt > 0$. Thus the agreement of the asymptotic values and the numerical computation is better than it seems at first glance.

4. Application to the analysis of shaped charges

We now apply the foregoing results to the description of the jet breakup in a conventional copper-lined conical-shaped charge. The present solution models the shaped-charge jet as a capillary inviscid liquid jet, thus essentially following the now classical approach of Birkhoff *et al.* (1948) who employed an ideal liquid as a model.

Let us first consider the effects on a perturbed jet with free surface described by

$$r = b = a(1+\eta\cos kz). \tag{39}$$

The liquid pressure changes due to the perturbation as:

$$P = \sigma\left(\frac{1}{R_1}+\frac{1}{R_2}\right) \cong \frac{\sigma}{b}\left(1-b\frac{\partial^2 b}{\partial z^2}\right).$$

Substituting b we thus obtain ΔF_S, the increment to the resultant tensile force on the perturbed capillary jet cross-section:

$$\Delta F_S \cong \pi a\sigma(1-k^2a^2)\,\eta\cos kz. \tag{40}$$

The only source of relevant data in the open literature are the studies of Carleone *et al.* (1977) and Chou *et al.* (1977). Carleone *et al.*, using a plastic flow model, obtained an expression for the average flow stress $\bar{y}$ (their equation 20). This, in present notation, is:

$$\bar{y} \cong y\left(1+\frac{b}{2}\frac{\partial^2 b}{\partial z^2}\right);$$

where y is the yield stress. Substituting b we obtain ΔF_p, the increment to the tensile force in the perturbed plastic jet:

$$\Delta F_p \cong 2\pi a^2 y(1-\tfrac{1}{4}k^2a^2)\,\eta\cos kz. \tag{41}$$

Thus, for ka sufficiently small, (40) and (41) are equivalent if the surface tension σ is equated to ya. We shall use this in order to be able to compare results.

The results in the literature show that decreasing the yield stress (surface tension) or increasing the density or the gradient of axial velocity all act to slow down the growth of perturbations in jets. All these effects are equivalent in the present solution to decreasing T, and thus it correctly predicts these tendencies.

We now select as a basis for comparison typical data for a shaped-charge jet (Chou & Carleone 1977): initial strain rate $K = 2.9\times10^4\ \mathrm{s}^{-1}$; initial radius $a_0 = 1.5$ mm; jet density $\rho = 8.9\ \mathrm{g/cm^3}$. We also take an average breakup time of $t_b = 75\ \mu\mathrm{s}$ (Chou *et al.* 1977).

From the above discussion we estimate: $\sigma \sim ya_0 = 3\times10^8\ \mathrm{dyn/cm}$ (taking $y = 2$ kbar as the plastic yield stress for copper). Thus we have: $T = 15.8$, $Kt_b = 2.18$. By interpolation in figure 7 we find $\chi_m \cong 0.33$.

Making use of these values together with the definitions of χ, $\bar{T}$ and (29) for χ_c, we calculate the appropriate values of k_0a_0 ($\cong 1.84$), $\bar{T}$ ($\cong 65.4$), χ_c ($\cong 0.992$) and hence estimate the time (associated with the instantaneous wavenumber χ_c) $t_c \sim 18\ \mu\mathrm{s}$. This time marks the beginning of divergence of the perturbation which dominates the breakup of the jet (cf. the paragraph after (31)). This result is confirmed by the numerical simulations of Chou *et al.* (1977) which also predict a finite time before amplification starts.

The value of χ_m enables also the estimation of the aspect ratio l/d (length to maximal diameter) of the segments of the broken jet, and the velocity difference ΔW between adjacent segments (both relatively simple for experimental measurement).

Assuming the perturbed surface to remain sinusoidal and the jet failure to occur when the absolute amplitude of the perturbation becomes equal to the radius of the jet, we obtain from conservation of volume:

$$\frac{l}{d} = \frac{\sqrt{6}\,\pi}{4\chi_m} = 5.92.$$

The velocity difference is obtained by calculating the wavelength of the perturbation prior to breakup and substituting in (3*a*). We find: $\Delta W = 149$ m/s.

These calculated values of l/d and ΔW are within the range of experimental data reported by Chou *et al.* (1977).

We finally examine F_b, the amplitude growth up to Kt_b, the non-dimensional breakup time. From figure 6 we see that, for $T = 10$, $Kt_b = 2.18$; $F_b \cong 3.5$. This unreasonably small value is probably a consequence of the above determination of σ (and hence of T) which is based on $y = 2$ kbar, the 'static' value for copper plastic yield stress.

Van Thiel & Levatin (1980) remark that they had to assume the plastic flow stress to be as high as $Y = 24$ kbar (instead of $y = 2$ kbar) in order to achieve a good agreement of their computations with experimental data for copper jets. In fact, it seems quite improbable that the 'static' value y could be applicable at the extremely high strain rates encountered in the shaped-charge jet.

The resemblance of the respective effects of ΔF_s and ΔF_p, (40) and (41), which was the basis for estimating σ, is independent of the specific value of y. Due to the uncertainty in Y, the determination of σ should at any rate be considered just as a crude order-of-magnitude estimate. If we thus take $T = 100$ (instead of 15.8) we obtain a more realistic value of $F_b = 500$ (cf. figure 6). This change in T causes only slight modifications in χ_m and l/d (as demonstrated in figure 7).

We thus conclude that the adjustment of the value of T (within the uncertainty range of Y) enables a complete simulation of shaped-charge-jet breakup.

5. Concluding remarks

The features of the present problem are best clarified through a comparison with the case of a non-stretching capillary jet (Rayleigh's solution): in the case of the non-stretching jet the wavelength of each perturbation is time independent. Consequently, perturbations exhibit either periodic oscillations (in the region of stable wavelengths) or simple exponential divergence (in the unstable region).

In the present problem the wavelength of each perturbation increases with time and therefore there is no simple exponential time dependence: a perturbation with a short initial wavelength starts as an oscillatory one with a moderate amplification and later becomes monotonically divergent (with a time-dependent growth rate).

Consequently, there is no one perturbation which dominates the whole process, but rather, the later the relevant time, the greater the amplification of the dominant perturbation and the shorter its initial wavelength.

The generalization of this solution to include the effect of the liquid viscosity is being presently accomplished and will be the subject of a forthcoming paper.

The discussion in §4 demonstrates that the present solution gives a good description of the essential features of the shaped-charge-jet breakup. Thus it may serve as a better insight into this phenomenon. The evaluation of this solution as an improved design tool depends on more detailed information than that to be found in the existing open literature.

Appendix A: The initial conditions for the numerical integration

Equation (20) is a second-order linear ordinary differential equation. Its general solution may be constructed by a linear combination of two linearly independent

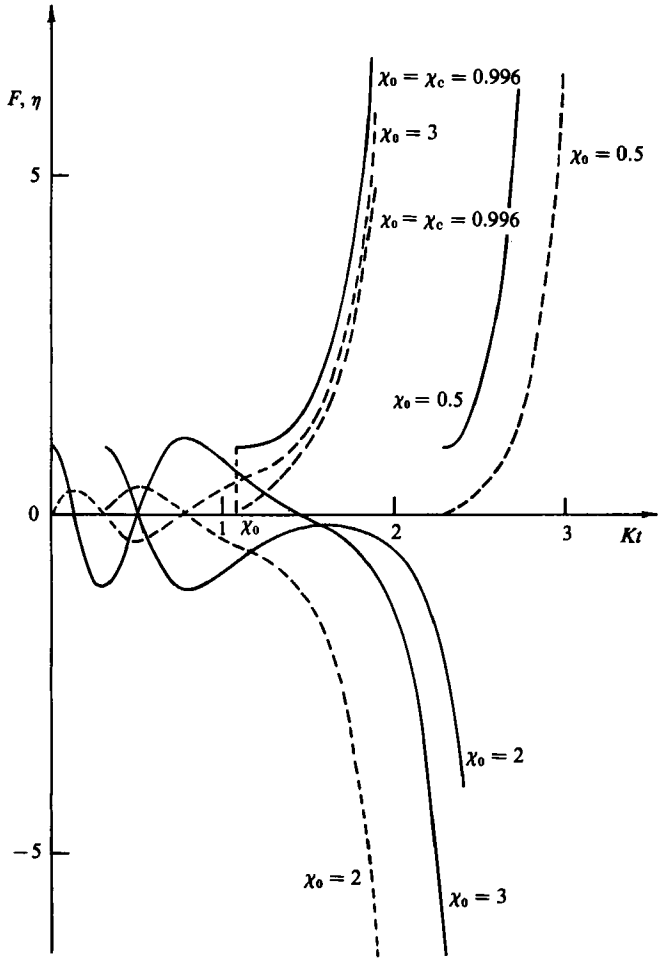

FIGURE 8. The influence of the initial conditions for $T = 10$, $k_0 a_0 = 3$, $\chi_0 = 3$, 2, 0.996, 0.5: ——, the solution F_1 which satisfies the initial conditions $\chi = \chi_0$; $F_1 = 1$, $F_1' = 0$; – – –, the solution F_2 which satisfies the initial conditions $\chi = \chi_0$; $F_2 = 0$, $F_2' = -k_0 a_0/\chi_0$.

solutions such as F_1 and F_2 which are obtained via integration of (20) together with the initial conditions:

$$\chi = \chi_0;\ F_1 \neq 0,\quad F_1' = 0; \tag{A 1a}$$

$$\chi = \chi_0;\ F_2 = 0,\quad F_2' \neq 0. \tag{A 1b}$$

The above discussion dealt exclusively with F_1. In the following we compare F_1 and F_2 in order to ensure that this choice does not conceal some essential features of the solutions of (20) (which may influence the physics of the present problem).

In describing F_1 we assumed that the initial relative amplitude was independent of χ_0. It thus seems reasonable to ascribe to F_2' an initial value such that the ratio of the perturbation of radial velocity and the radial velocity of the free surface of the jet is independent of χ_0.

According to the kinematic boundary condition, (10), $u/U_0 \sim O(a\eta'/a')$. Substituting $a(t)$ from (4), we obtain the appropriate initial condition:

$$\chi = \chi_0;\ F_2' = -\frac{k_0 a_0}{\chi_0}. \tag{A 2}$$

Figure 8 examines the effect of the initial conditions through comparison of F_1, F_2. (The curves of F_2 were added to figure 3 which had originally contained only the curves of F_1.) No essential differences are revealed by comparison of the two families of curves.

Appendix B: The divergence of perturbations for $\chi_0 < \chi_c$

We write (18) in short:

$$\eta'' + b(t)\,\eta' - c(t)\,\eta = 0; \tag{B 1}$$

where $c(t) > 0$ and $b(t)$ is non-singular.

Multiplying this equation by $\exp[\int_{t_0}^{t} b(\tau)\,\mathrm{d}\tau]$ we obtain the self-adjoint form:

$$\frac{\mathrm{d}}{\mathrm{d}t}\,\eta' \exp\left[\int_{t_0}^{t} b(\tau)\,\mathrm{d}\tau\right] = c(t) \exp\left[\int_{t_0}^{t} b(\tau)\,\mathrm{d}\tau\right]\eta$$

and integrating together with the initial conditions $t = t_0$; $\eta = 1$, $\eta' = 0$, (27):

$$\eta'(t) = \int_{t_0}^{t} c(\tau_1)\,\eta(\tau_1) \exp\left[-\int_{\tau_1}^{t} b(\tau)\,\mathrm{d}\tau\right]\mathrm{d}\tau_1. \tag{B 2}$$

Since $\eta(t_0) = 1$, $\eta > 0$ for some interval $t_0 < t < t_1$. Then from (B 2) $\eta'(t) \geqslant 0$ and monotonically increasing; hence $\eta(t)$ is also monotonically increasing and $\eta(t_1) > \eta(t_0) > 0$. We may thus repeat this process for some interval $t_1 < t < t_2$ and so forth. Therefore η, η' are both monotonically divergent provided that $\chi_0 < \chi_c$.

REFERENCES

Birkhoff, G., MacDougall, D. P., Pugh, E. M. & Taylor, G. I. 1948 Explosives with lined cavities. *J. Appl. Phys.* **19**, 563–582.

Bogy, D. B. 1979 Drop formation in a circular liquid jet. *Ann. Rev. Fluid Mech.* **11**, 207–228.

Carleone, J., Chou, P. C. & Ciccarelli, R. D. 1977 Shaped charge jet stability and penetration calculations. *BRL-CR*-351.

Chou, P. C. & Carleone, J. 1977 The stability of shaped charge jets. *J. Appl. Phys.* **48**, 4187–4195.

Chou, P. C., Carleone, J., Tanzio, C. A. & Ciccarelli, R. D. 1977 Shaped charge jet breakup studies using radiograph measurements and surface instability calculations. *BRL CR*-337.

Dipersio, R., Simon, T. & Martin, T. H. 1960 A study of jets from scaled conical shaped charge liners. *BRL-MR*-1298.

Eichelberger, R. J. 1956 Experimental test of the theory of penetration by metallic jets. *J. Appl. Phys.* **27**, 63–68.

Frankel, I. 1984 Flow and stability in liquid jets with a longitudinal distribution of axial velocity. D.Sc. thesis, Technion.

Goldin, M., Yerushalmi, J., Pfeffer, R. & Shinnar, R. 1969 Breakup of a laminar capillary jet of a viscoelastic fluid. *J. Fluid Mech.* **38**, 689–711.

Lamb, H. 1932 *Hydrodynamics* (6th edn). Cambridge University Press. (Reprinted by Dover, 1945.)

Levich, V. G. 1962 *Physicochemical Hydrodynamics*. Prentice-Hall.

Mikami, T., Cox, R. G. & Mason, S. G. 1975 Breakup of extending liquid threads. *Intl J. Multiphase Flow* **2**, 113–138.

Murray, J. D. 1974 *Asymptotic Analysis*. Clarendon.

Pugh, E. M., Eichelberger, R. J. & Rostoker, N. 1952 Theory of jet formation by charges with lined conical cavities. *J. Appl. Phys.* **23**, 532–536.

Rayleigh, Lord 1894 *The Theory of Sound* (2nd edn). (Reprinted by Dover, 1945.)

Shelton, R. D. & Arbuckle, A. L. 1979 A calculation of particle size distribution in the breakup of shaped charge jets. *J. Appl. Phys.* **50**, 6190–6195.

TOMOTIKA, S. 1936 Breaking up of a drop of viscous liquid immersed in another viscous fluid which is extending at a uniform rate. *Proc. R. Soc. Lond.* A **153**, 302–318.

VAN THIEL, M. & LEVATIN, J. 1980 Jet formation experiments and computations with a Lagrange code. *J. Appl. Phys.* **51**, 6107–6114.

WEBER, C. 1931 Zum Zerfall eines Flüssigkeitsstrahles. *Z. angew. Math. Mech.* **11**, 136–154.